Integrated geophysical Investigations for Archaeology
EAGE Journal

Archaeological Investigations in the Shallow Seawater Environment with Electrical Resistivity Tomography

Kleanthis Simyrdanis *[1], Nikos Papadopoulos [1], Jung-Ho Kim[2], Panagiotis Tsourlos[3], Ian Moffat[1]

[1] Laboratory of Geophysical-Satellite Remote Sensing, Institute for Mediterranean Studies, Foundation for Research & Technology-Hellas (F.O.R.T.H.), Rethymno, Greece; ksimirda@ims.forth.gr
[2] Korea Institute of Geoscience and Mineral Resources (KIGAM), Korea
[3] Department of Geophysics, School of Geology, Aristotle University of Thessaloniki

ABSTRACT

This work explores the applicability and effectiveness of Electrical Resistivity Tomography (ERT) in mapping archaeological relics in the shallow marine environment. The approach consists of a methodology based on numerical simulation models validated with comparison to with field data. Numerical modeling includes the testing of different electrode arrays suitable for multichannel resistivity instruments (dipole-dipole, pole-dipole, gradient). The electrodes are placed at fixed positions either floating on the sea surface or submerged at the bottom of the sea. Additional tests are made concerning the resolving capabilities of ERT with various seawater depths and target characteristics (dimensions and burial depth of the targets). Although valid 'a priori' information, in terms of water resistivity and thickness, can be useful for constraining the inversion, it should be judiciously to prevent erroneous information leading to misleading results. Finally, an application of the method at a field site is presented not only for verification of the theoretical results but at the same time for proposing techniques to overcome problems that can occur due to the special environment. Numerical and field ERT results indicated the utility of the method in reconstructing off-shore cultural features, demonstrating at the same time its applicability to be integrated in wider archaeological projects.

INTRODUCTION

During recent years there has been an increasing trend of employing the electrical resistivity method for off-shore applications and, in particular, the use of two dimensional (2D) electrical resistivity tomography (ERT) in water-covered areas (Wynn and Grosz 2000). ERT has been used: for mapping geological formations (Rucker et al. 2011), to image the geological stratigraphy beneath water covered areas for tunnel and bridge construction projects on river or lake sites (Kwon et al. 2005, Kim et al. 2002; Allen, 2007; Colombero et al. 2014) and for the geotechnical characterization of the submerged subsurface prior to a port construction (Apostolopoulos, 2012). Marine ERT surveys have been also used to characterize the waterbed sediments (Orlando, 2013) or for mapping the beachrock (Psomiadis et al., 2009). Non-conventional underwater geoelectrical surveys have also been proposed for mapping lake-bottom geology in water depths exceeding 100m (Baumgartner and Christensen 1998).

In contrast to the previous applications, the use of electrical resistivity method is uncommon in submarine archaeology and only limited studies have been presented (Passaro, 2010). ERT data acquisition is accomplished through a fixed cable that can float on the water surface or can be submerged in the sea bottom. These marine surveys can be undertaken with standard resistivity meters. The main challenge for mapping the subsurface stratigraphy in marine environments is the highly conductive nature of the seawater in comparison with the resistive sediments (Lagabrielle, 1983). However there are some issues that need to be solved concerning the installation of the electrodes and the most appropriate modeling and inversion approaches to cope with the special conditions that are found in such environments (Loke and Lane 2004).

This study investigates the efficiency of ERT for mapping archaeological relics buried beneath the sediment-water interface in shallow marine environments. In order to undertake a thorough study of an archaeological survey in this environment, extensive testing was performed with numerical modeling and synthetic data. Initially, different electrode arrays were tested in order to determine the most efficient one for such surveys. Data acquired using floating or submerged electrodes were compared and 'a priori' information during the inversion procedure was introduced taking into consideration the water depth and the resistivity of the seawater. Additional tests were undertaken to determine the ERT horizontal and vertical resolving capabilities. Finally, a case scenario is presented from an archaeological site in the island of Crete, in an effort to validate the numerical results.

METHODOLOGY

The 2D ERT numerical experiments were performed with a proven 2D forward and inversion algorithm ('DC2DPro' by Kim and Yi, 2010). The program is based on a 2.5D finite element routine to solve the forward resistivity problem and an iterative least squares algorithm with Active Constrain Balancing (ACB) for reconstructing the subsurface resistivity models.

A typical resistivity model that is used for the numerical simulations is shown in Figure 1. The number of the electrodes is 48 with the probe spacing set to a=1m. Both cases with floating (indicated with black dots) and submerged (indicated with white dots) position of the electrodes are tested. The seawater resistivity value is defined to ρ_{water}=0.2 ohm-m and for the homogeneous medium below sea bottom is set to ρ_{back}=10 ohm-m. Furthermore, the thickness of the column of the sea is set to D=1m for most of the cases, except when the effect of the column thickness is studied, in which case different depths are introduced. A resistive target with ρ_{target}= 500 ohm-m is used to simulate an archaeological structure (e.g. wall). The dimension of the target is 5x2m in all cases except when the resolving ability of the arrays is tested and thus different target sizes are used.

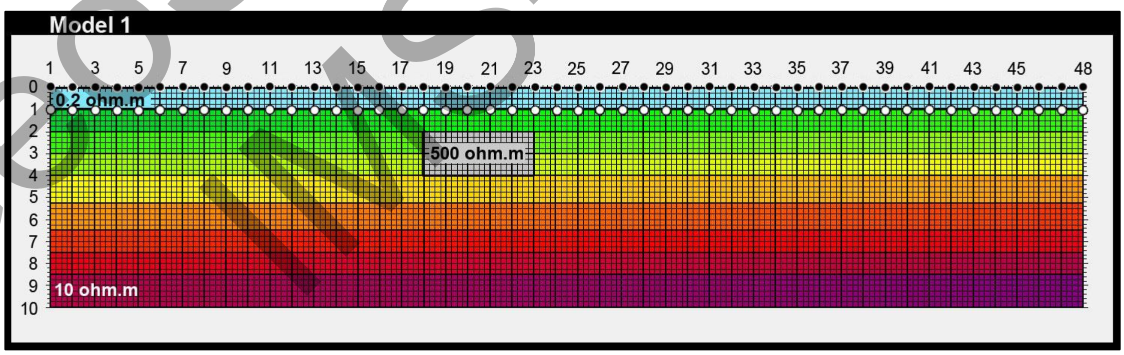

Figure 1. Synthetic model 1 for comparing different protocols using floating (black dots) and submerged (white dots) electrodes. Water depth D=1m, ρ_{water}= 0.2 ohm-m, ρ_{target}= 500 ohm-m, ρ_{back}= 10 ohm-m. Electrode spacing is set to a=1m.

Different electrode arrays (Figure 2a, b and c), mainly suitable for multichannel resistivity meters, like: dipole-dipole ('dd'), gradient ('grd') and pole-dipole ('pd') were tested. All pole-dipole arrays include the combination of forward and reverse measurements with the electrode B placed at a practically infinite distance (e.g. more than 10 times the largest distance between A and M electrodes. Electrode maximum separation distance is N=7a for dipole-dipole and pole-dipole and N=20a for gradient array. The separation between A-B and M-N electrodes was increased from 1a to 5a ('a' the electrode spacing) in an effort to increase the signal to noise ratio. Synthetic data were corrupted with gaussian noise of ±0.05mV/V into the potential values in order to better simulate a real case scenario.

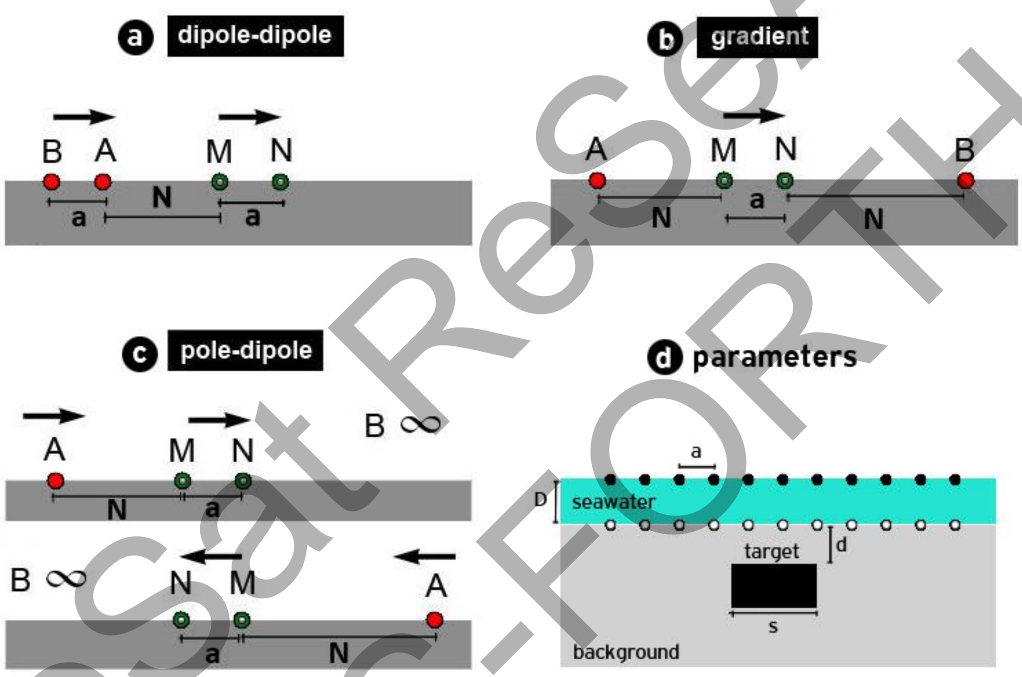

Figure 2. Electrode arrays used for marine ERT measurements (a, b and c). For the pole-dipole the forward and reverse modes were used to create the measurement protocols. Electrodes A and B are used to inject the current. The potential difference is measured in M and N electrodes. At the bottom right side, the parameters that are used are depicted (d).

Since the whole marine survey is done in a shallow water environment it is straight forward to obtain the water depth and measure the resistivity of the seawater. This data can be introduced during the inversion procedure as 'a priori' information so as to constrain the inversion. The 'a priori' information is used either by introducing a variable weighting value on the resistivity values of the parameters that correspond to the water layer (Kim et al., 2014) or by fixing the respective parameter resistivity values throughout the inversion procedure. The variable weighting starts with an initial value and decreases at each iteration of the inversion. For the specific study the initial value was set to 0.2, after numerous trial and error testing. Additional cases with erroneous 'a priori' information were also tested by over or under estimating the true value of the water resistivity and thickness. At the same time the water depth ('D') is a significant factor regarding the resolving capability of the arrays due to the absorption of the current energy from the conductive sea layer. For this reason, different water depths are tested (Figure 2d), as well as different depths 'd' of the target itself below sea bottom. In all synthetic models the inversion algorithm was terminated after 7 iterations unless some other criteria were met (e.g. slow convergence rate of less than 3%, rms error smaller than the noise level).

NUMERICAL SIMULATIONS

Efficient protocols and Floating vs. Submerged electrodes

Synthetic Model 1 (Figure 1) is used for comparison between the arrays dipole-dipole ('dd'), pole-dipole ('pd') and gradient ('grd') as well as the floating (indicated by black dots) and submerged (indicated by white dots) modes for the electrodes' layout. The final resistivity models in these cases resulted without adding any 'a priori' information in the inversion procedure.

Regarding the floating electrode mode and a water depth of D=1m, 'dd' array is not able to reconstruct the target satisfactorily since some distortions appear below the target, transforming its original shape (Figure 3, left panel). On the contrary 'pd' and 'grd' arrays have better inversion results regarding the shape of the target. Both 'pd' and 'grd' arrays have smaller rms error ('pd': 0.56%, 'grd': 0.44%) in comparison to the 'dd' array ('dd': 1.51%).

When using the submerged electrodes, the shape of the target is slightly better reconstructed by 'dd' and 'grd'. The 'pd' submerged inversion model shows a slight vertical distortion of the target. However in all cases the original position of the resistive prism is vertically downward shifted (Figure 3, right panel). At the same time it can be observed that the floating electrode configuration produces higher resistivity values, in comparison with the submerged ones.

All the models in Figure 3 show some artifacts as resistive regions that appear close to the edges of the inversion images. This is attributed to the large resistivity contrast between the highly conductive seawater layer and the less conductive background. The numerical limitations of the modeling and inversion procedures cannot efficiently cope with this two orders of magnitude resistivity contrast. During inversion procedure, the lack of ability to match the theoretical with the corrected apparent resistivity values at each iteration leads to the appearance of those artifacts. Extensive testing (not shown here) with smaller resistivity contrasts between the seawater and background layers eliminated these inversion artifacts.

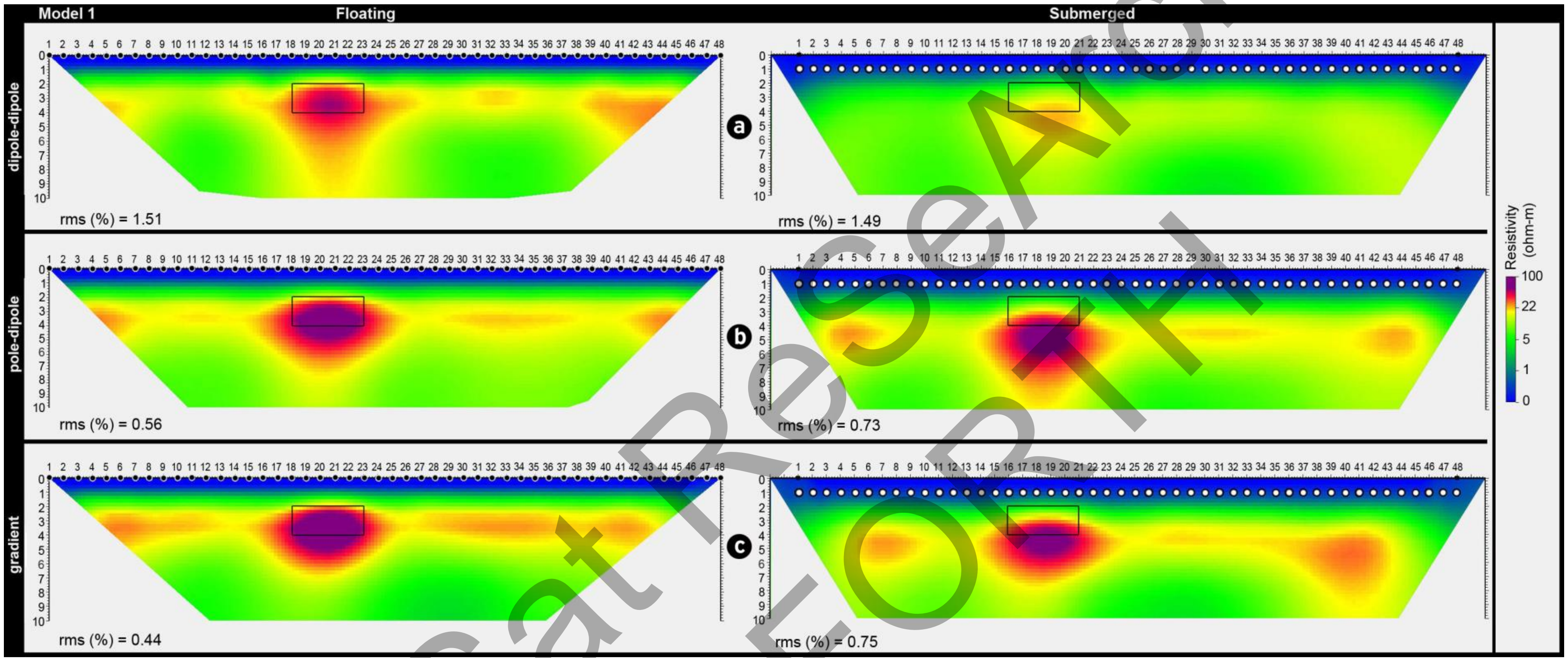

Figure 3. (Model 1) Inversion results with different protocols (a) dipole-dipole, (b) pole-dipole and (c) gradient using 48 floating (black dots, left), submerged (white dots, right) electrodes with spacing a=1m. Water depth is set to D=1m.

Effect of Water Depth (D)

Accurate constraint of water depth (D) is crucial for the marine investigation, since seawater is a very conductive medium and is responsible for severe current attenuation. Towards this direction, Model 2 (Figure 4, left panel) was constructed in order to investigate the maximum water depth, to which ERT would be effective in locating isolated resistive targets. The resistive prism with dimensions of 5m by 2m was placed at a depth of 2m below the sea surface. The cases of increasing thickness of the conductive water were evaluated (Figure 4a, b, c) and the respective final inversion models resulted without imposing any 'a priori' information within the inversion procedure.

In this case a 'pd' protocol was used for three different water depth values (a) D=0.5m, (b) 1m and (c) 2m and the 2D inversion results are shown in Figure 4 (right panel). The reconstructed resistivity sections signify that the resolving capabilities of floating ERT survey mode, in terms of mapping isolated targets, are constrained from the seawater layer thickness. If the seawater layer exceeds the thickness of 1m it is impossible to reconstruct the isolated archaeological resistive body and the tomographic image retrieves information only for the horizontal stratigraphy and the transition from the sea to the background layer (Figure 4c). Additionally, more artifacts appear as the seawater thickness increases. It should be noted that, when the water layer thickness is set to D=0.5 m (Figure 4a), there are less artifacts on the inversion result.

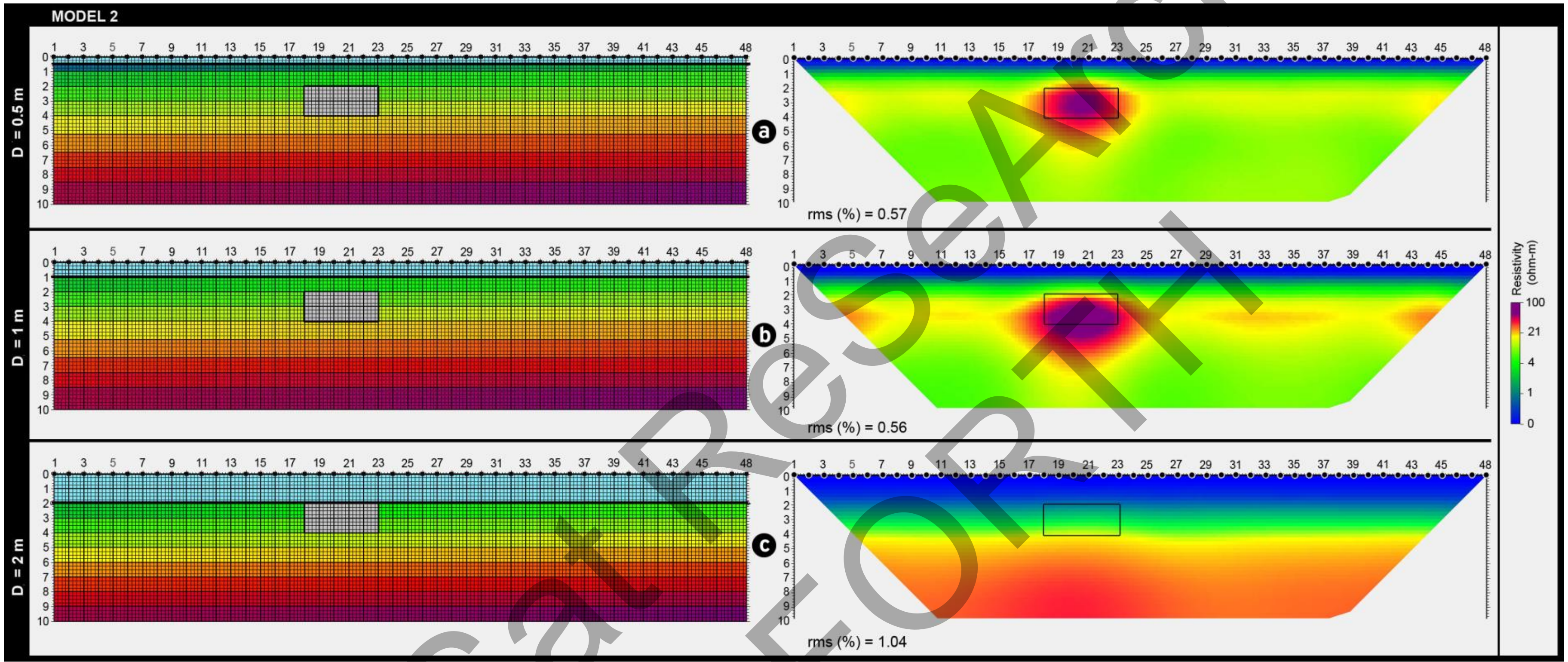

Figure 4. (Model2) Synthetic model for comparing different water depth using protocol pole-dipole with floating (black dots) electrodes. Water depths: (a) D1=0.5m, (b) D2=1m and (c) D3=2m, ρ_{water}= 0.2 ohm-m, ρ_{target}= 500 ohm-m, ρ_{back}= 10 ohm-m, electrode spacing a=1m (left). 2-D inversion results (right).

Location and Dimension of the Targets

The nature of the isolated archaeological target itself is a crucial factor that should be considered during marine investigations. For that purpose, extra models were created regarding (a) the burial depth of the target below the bottom of the sea (Figure 5) and (b) the size of the target (Figure 6). Both floating and submerged electrodes are used. In the specific numerical experiments the option of using 'a priori' information was enabled for the case of submerged electrodes.

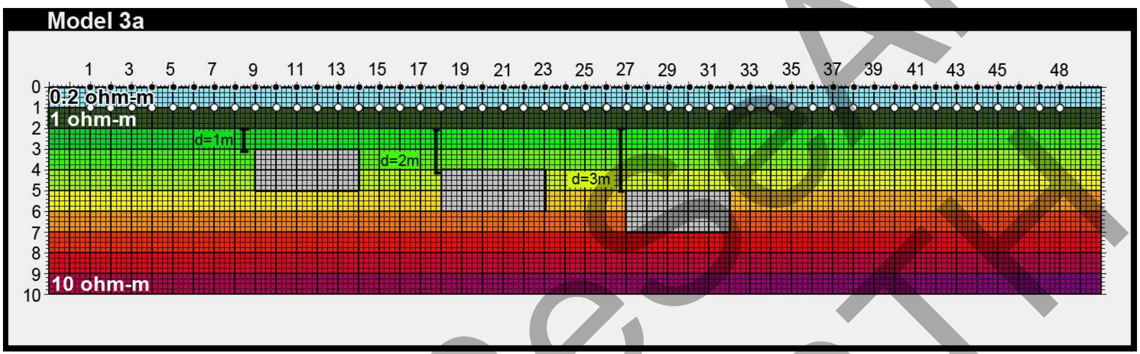

Figure 5. Synthetic Model 3a for studying different target burial depths (d=1m, 2m and 3m) of three resistive targets using different protocols with floating (black dots) and submerged (white dots) electrodes. Water depth D=1m, ρ_{water}= 0.2 ohm-m, ρ_{target}= 500 ohm-m, ρ_{back}= 10 ohm-m. Overburden layer 1m thick with ρ_{ob}=1 ohm-m. Electrode spacing a=1m.

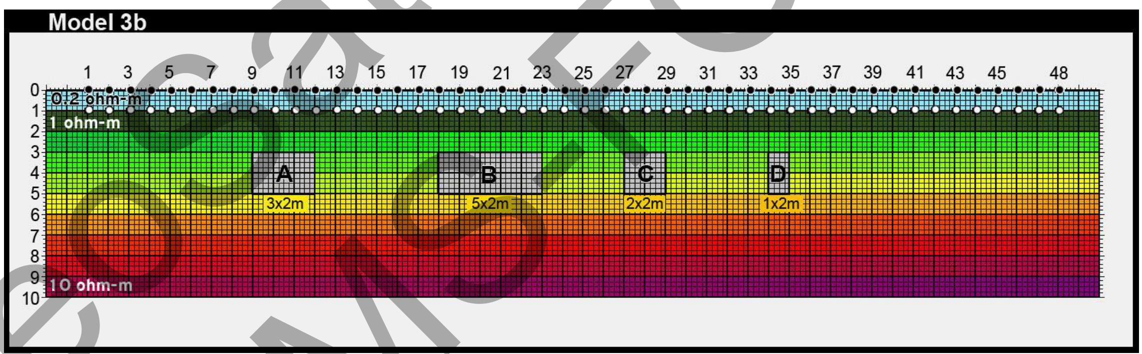

Figure 6. Synthetic Model 3b for studying different target sizes (A, B, C and D) of resistive targets using protocol pole-dipole with floating (black dots) and submerged (white dots) electrodes. Water depth D=1m, ρ_{water}= 0.2 ohm-m, ρ_{target}= 500 ohm-m, ρ_{back}= 10 ohm-m. Overburden layer 1m thick with ρ_{ob}=1 ohm-m. Electrode spacing a=1m.

The top row of Figure 7a shows that the 'dd' protocol is not able to detect the targets when they are buried more than 2m below the sea bottom in the presence of the extra conductive layer (overburden). This happens regardless the survey mode (floating or submerged). Once more, the inverted resistivity values of the submerged mode of 'dd' protocol are smaller than the respective values of the floating mode results. On the other hand, 'pd' and 'grd' are more successful in outlining the different targets, with the 'pd' giving slightly superior results both for the floating and submerged survey modes, as the targets can be more clearly distinguished (Figure 7b, c). As it was expected the submerged 'pd' and 'grd' surveys were able to reconstruct the deeper buried targets with greater clarity than the floating one. At the same time the incorporation of the 'a priori' information within the inversion procedure minimized the downward shifting of the targets as well as the spurious effects at the edges of the inversion images.

In Model 3b (Figure 8) the horizontal resolving capability of the 'pd' array, in floating and submerged modes, is examined for the reconstruction of resistive bodies with similar resistivity values (500 ohm-m) but different dimensions. In general, the smaller bodies (C and D) aren't outlined by the floating survey mode and only the body C is faintly reconstructed by the submerged survey mode. The larger targets A and B are better reconstructed with both survey modes in relation to targets C and D. At the same time the resistivity images show the superiority and the higher resolving capabilities of the submerged ERT survey mode for outlining isolated targets in cases of complicated subsurface stratigraphy.

A significant number of synthetic modeling experiments were completed with multiple combinations of the basic probe spacing ('a'), the water depth ('D'), the burial depth ('d') and the size ('s') of the isolated targets. This extensive testing suggested a first order generalization regarding the optimum survey strategy that could be employed in real situations. Thus an effective ERT shallow marine survey should employ a probe spacing half the smallest target dimension ($a \leq s/2$). For example, if we are trying to locate a wall with 2 meters horizontal dimension, the probe spacing should not be more than 1m. The basic electrode distance ('a') has to be less or equal the water depth ('D') regarding floating survey modes for successfully mapping isolated targets. If a greater electrode spacing greater than the water depth must be used, the submerged ERT survey mode is more appropriate. Furthermore, depending on the electrode configuration (Figure 7b, c) the ERT inversion image can reconstruct targets that are buried even at a depth below the bottom of the sea five times larger than the water depth. It seems that pole-dipole and gradient arrays, both in floating and submerged survey modes, show strong resolving capabilities that can be used for the efficient mapping of submerged cultural objects (Figure 7b and c). On the other hand dipole-dipole protocols show significant deficiency in outlining isolated targets in the shallow marine environments.

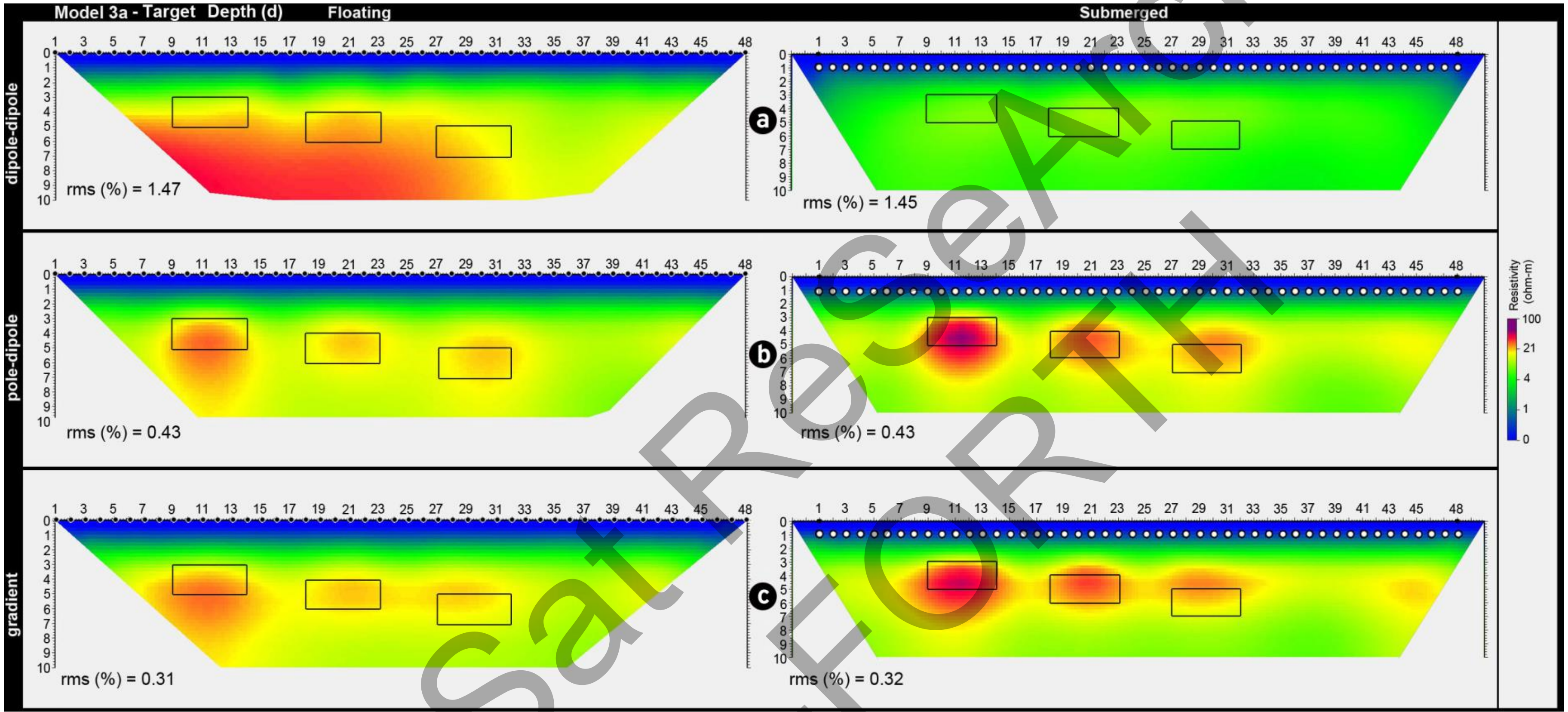

Figure 7. (Model 3a) Inversion results for studying target depth with different protocols (a) dipole-dipole, (b) pole-dipole and (c) gradient using 48 floating (left) and submerged(right) electrodes with spacing a=1m.

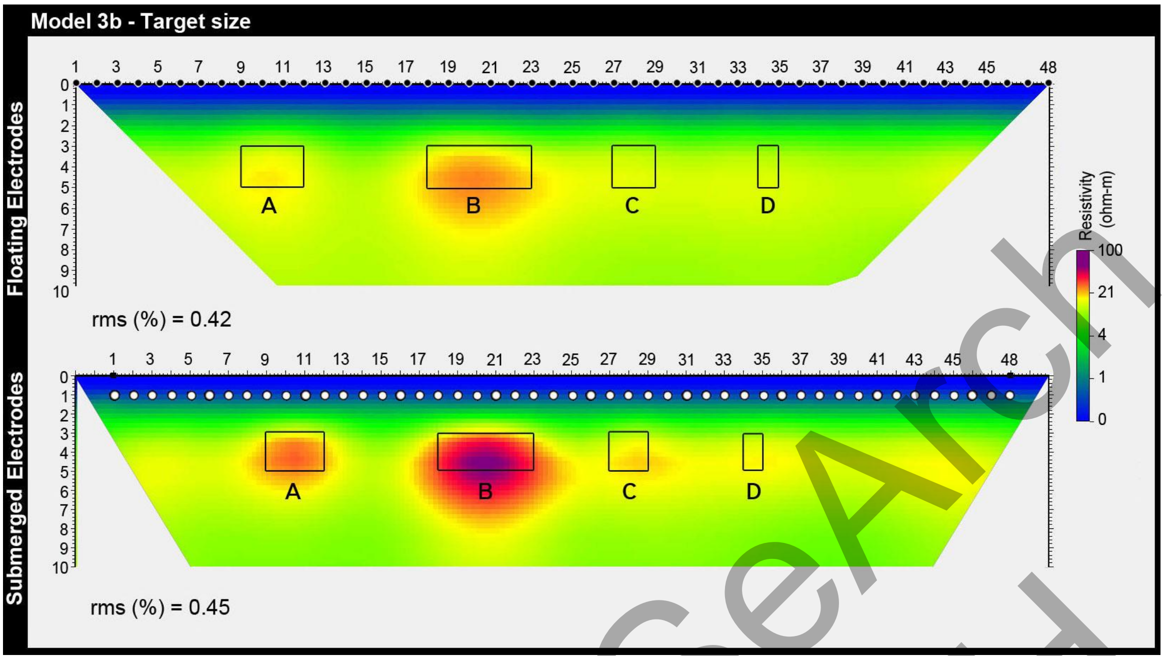

Figure 8. (Model 3b) Inversion results with protocol pole-dipole using floating (top) and submerged (bottom) electrodes with spacing a=1m.

Effect of erroneous 'a priori' information

'A priori' information plays a significant role in the successful imaging of the subsurface in marine environments. In case of invalid 'a priori' information, erroneous inversion results may occur. To test this hypothesis Model 4 is created (Figure 9, top left) where only submerged electrodes were used. The electrode spacing is set to a=1m, a new target (7x2m) is used (ρ=500 ohm-m) which is placed at the depth of 2m below the seawater surface at all cases and the chosen array is pole-dipole. Initially, as shown in Figure 9a, an inversion was made where the correct values of seawater depth and resistivity value are set. This inversion image was used as a reference for comparison with the following tests where erroneous water depth (Figure 9b, c) or resistivity values (Figure 9d, e) were introduced to the inversion procedure.

Under-estimating (Figure 9b) or over-estimating (Figure 9c) the correct water depth has serious effects in the final resistivity image since the resistive target can not be outlined in either cases. Similar distortions appear when assigning erroneous information for the seawater resistivity. Underestimating the seawater resistivity value (Figure 9d) results in the failure of the method to locate the target, regardless the applied resistivity scale. The overestimation of the resistivity value (Figure 9e) forces the target to be shifted vertically downwards. These tests clearly demonstrate the importance of incorporating valid information for the water depth and its resistivity within the inversion procedure in order to reconstruct resistivity models that correspond to reality and the actual subsurface conditions.

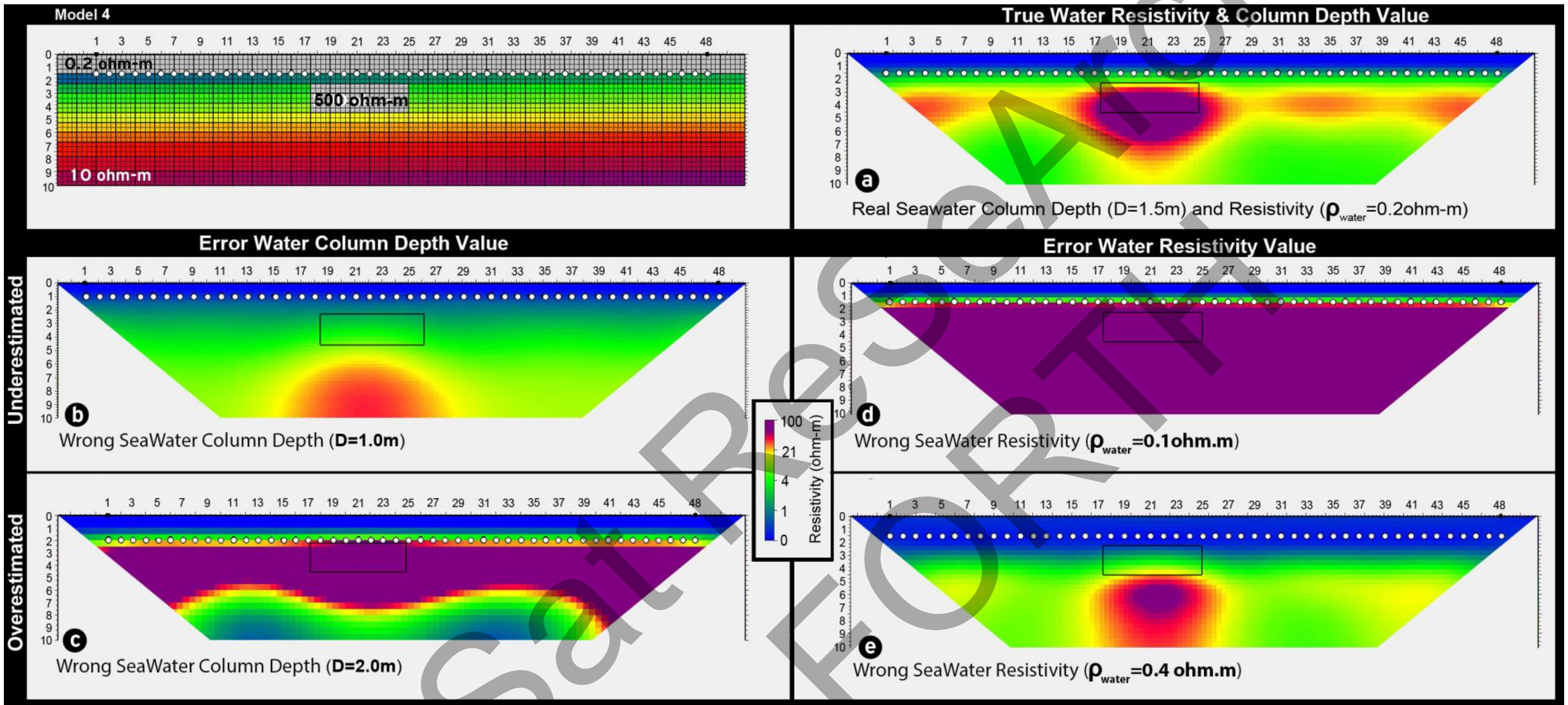

Figure 9. Synthetic Model 4 for studying erroneous 'a priori' information (over- or under-estimated) using protocol pole-dipole with submerged (white dots) electrodes. True water depth is D=1.5m and real resistivity value is ρ_{water}= 0.2 ohm-m, ρ_{target}= 500 ohm-m, ρ_{back}= 10 ohm-m. Electrode spacing a=1m.

FIELD CASE STUDY

The first attempts at employing the ERT in a marine archaeological area were undertaken in the littoral archaeological site of Agioi Theodoroi in Crete (Greece). The experimental ERT survey was integrated in a wider project aiming to reconstruct and understand the past cultural dynamics of the specific site. The initiative includes the employment of geoinformation technologies like GPS mapping and aerial photography for documenting the visible and submerged archaeological material.

The coastal archaeological area of Agioi Theodoroi is located about 10 km east of the city of Heraklion in Crete, Greece (Figure 10). The area was subject to systematic excavations during the early 20th century that revealed the existence of seaside buildings and wall constructions that continue towards the sea, dating since the Minoan Times (Marinatos, 1926). Recent archaeological surveys included the mapping and photo capturing of the submerged structural relics with underwater camera (Figure 10).

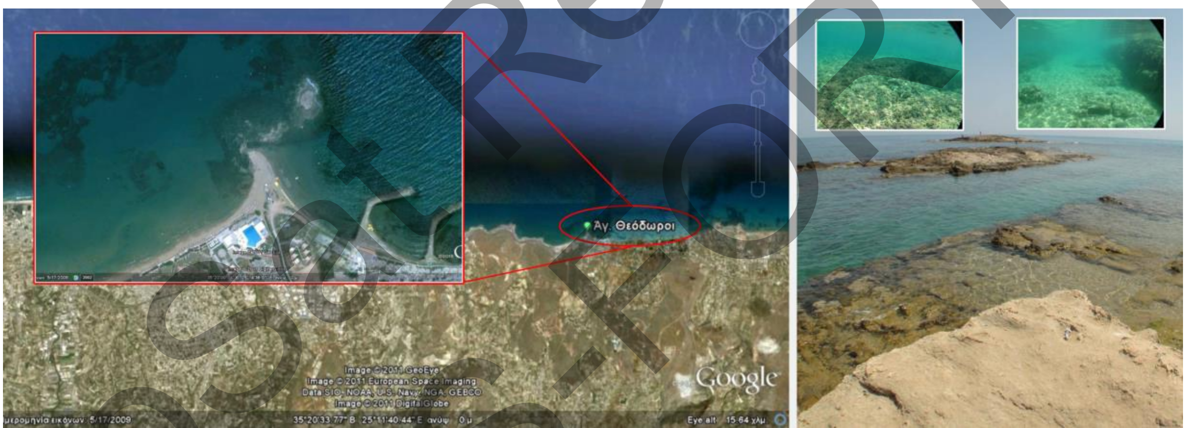

Figure 10. Site for marine investigation and archaeological targets (Heraklion, Crete).

In order to complete the wider picture of the visible on-shore and off-shore relics, a high resolution aerial photography survey was undertaken using standard photo camera mounted on a kite. The photographs were taken at an altitude of between 50 and 100 meters using an exposure time of 1/1000 sec and an ISO of 160 at a time increment of every five seconds. In total, 172 photos were selected for inclusion in the final model and combined into a composite orthophoto using a commercial software (Agisoft Photoscan). The orthophoto was georectified to Universal Traverse Mercator Reference System using ground control points collected with a differential GPS. The location of the visible relics was also mapped with the same GPS unit. The orthophoto (Figure 11) was used as a base map for plotting the position of the underwater features which were recorded during fieldwork as well as the location of ERT line. This combined plan allowed the direct comparison between the geophysical results, archaeological features and the survey area during data processing and interpretation.

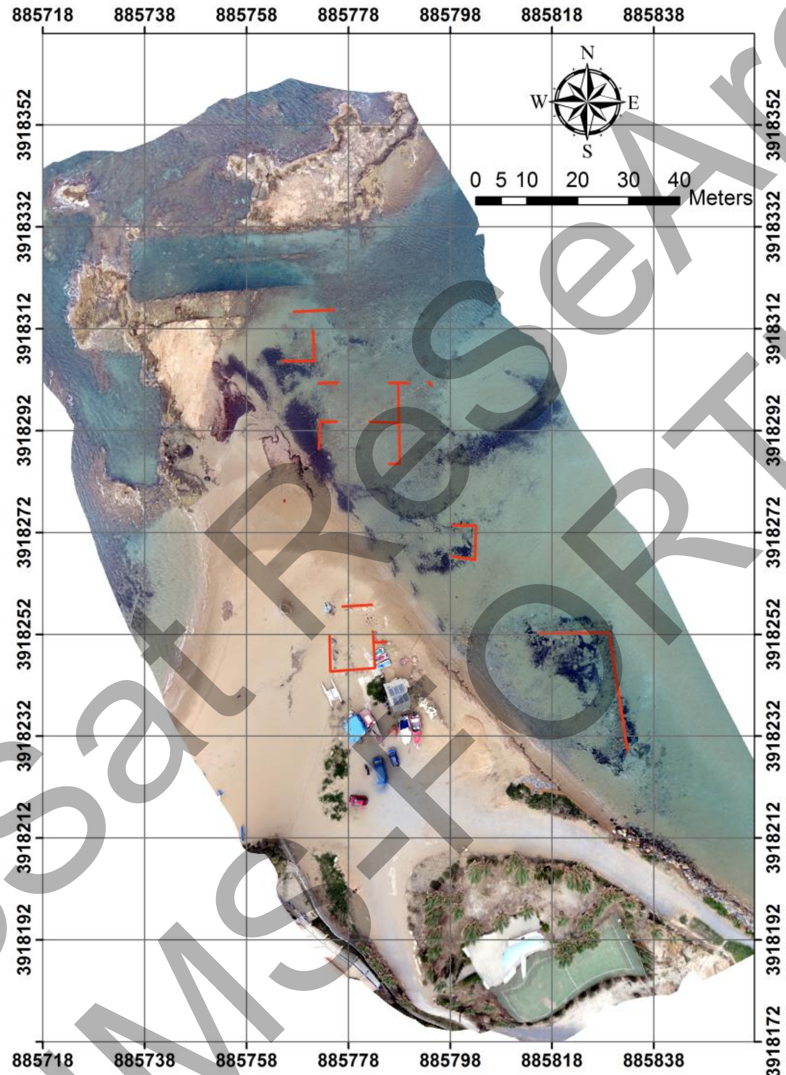

Figure 11. Aerial photo of the survey area in Agioi Theodoroi. The red lines indicate the location of the on-shore and off-shore archaeological relics that were visible from the aerial photo and those mapped with the differential GPS system.

To validate the efficiency of marine resistivity archaeological investigations in field situations ERT Line 1 was laid out in a southwest-northeast direction running for a total length of 24 meters (Figure 12). The first electrode was submerged into the water at a distance of 1 meter away from the shoreline. The line was composed of 25 electrodes equally spaced every 1 meter. A 10-channel resistivity meter and a multimode marine cable composed of stainless steel cylindrical electrodes were used for the data capturing. The same cable was used for floating and submerged electrode position modes.

Protocols dipole-dipole, pole-dipole and gradient were used with maximum separation N=8a and 1a, 2a and 3a (where ‘a’ is the electrode spacing). For the pole-dipole array, the “B” electrode (‘infinite’) was set at a distance of more than 150m away in a SE direction and perpendicular to direction of the survey line and embedded inside the sea. To ensure that it didn’t move during the survey it was stabilized with a heavy rock.

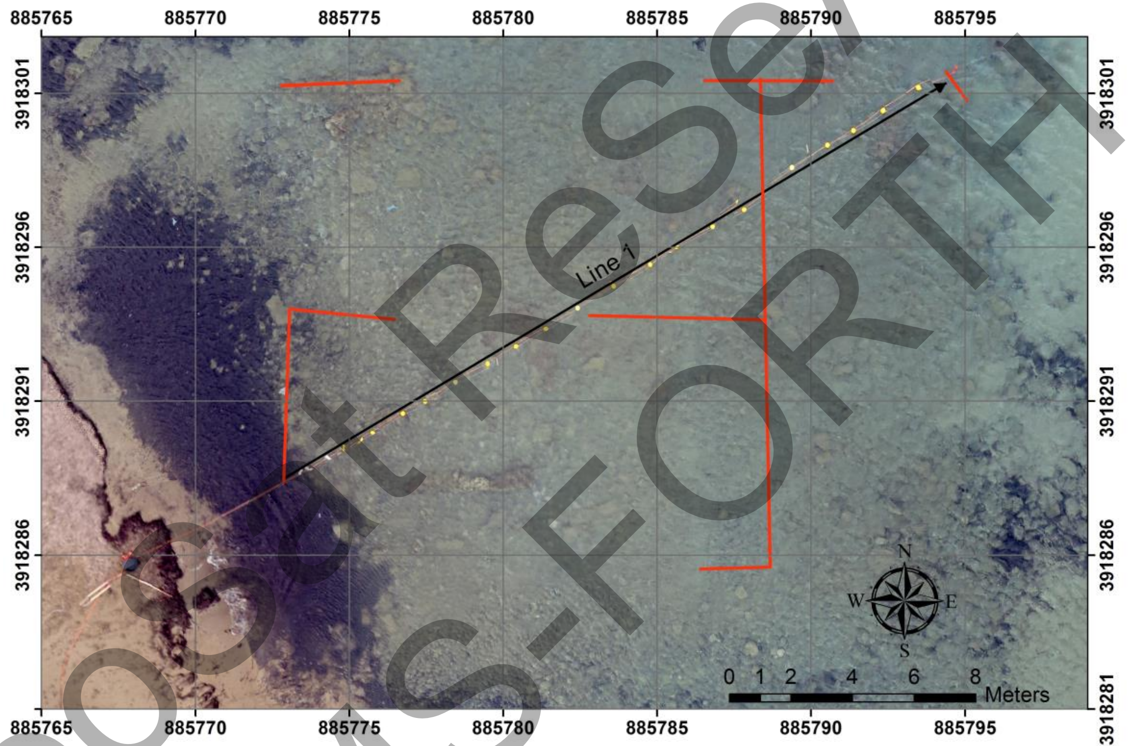

Figure 12. Outline of the Line 1 that was used to validate the efficiency of ERT underwater survey. The yellow dots show the floaters that were used in every electrode position to keep the cable floating. The red lines outline the submerged archaeological relics that were mapped.

The ERT line crossed over three known walls whose position has already been identified by field observations and mapped with the differential GPS. Specifically, electrodes ‘3’, ‘4’, ‘13’, ‘14’, ‘15’ and ‘21’, ‘22’ were exactly above the wall relics as shown in Figure 12. For the floating survey mode long wooden sticks were embedded in bottom of the sea at the beginning and at the end of the survey line to keep the cable fixed and steady during the measurements. Plastic bouys were tied along the cable to faciliate the floating of the electrodes (Figure 13). During the submerged mode, rocks were placed along the cable between the electrodes to ensure it remained stationary on the sea floor.

A hand held conductivity meter was used to measure the seawater resistivity at least 5 different points along the line which had an average value 0.19 Ohm-m with temperature 22.4^{o}C. The water depth was measured at each probe position, using a plastic calibrated stick of 2m length in total (Figure 13, embedded photo top right). The water depth values deepened from 46cm to 96cm away from the shoreline. This information was later incorporated into the inversion procedure.

Figure 13. Photo with floating electrodes set up, equipment used (embedded bottom left), water depth calculation with a plastic calibrated stick (embedded up right).

As it was expected, very low potential values were measured with all the arrays due to the conductive environment. After potential normalization with corresponding current values the corresponding histograms for the field measurements of each array (dipole-dipole, pole-dipole and gradient) are shown in Figure 14. Values for floating electrodes are colored blue and for submerged ones are colored red. The basic statistical analysis of the normalized potential values regarding the minimum, maximum and average values are shown in Table 1. Floating and submerged survey modes for all the arrays show comparable signal. However dipole-dipole has the lowest signal compared to pole-dipole and gradient, reflects the inversion results shown in the respective numerical modeling examples. On the other hand, pole-dipole and gradient protocols exhibit stronger signal which, in turn, is attributed to the more resolvable resistivity inversion models.

Normalized potential values	Dipole-Dipole		Pole-Dipole		Gradient	
	Floating	Submerged	Floating	Submerged	Floating	Submerged
MIN	0.0004	0.0003	0.0019	0.0019	0.003	0.0029
MAX	0.0477	0.0453	0.0737	0.0678	0.0718	0.0763
AVERAGE	0.0064	0.0060	0.0132	0.0127	0.0186	0.0175

Table 1. Normalized potential values (min, max and average) for all arrays and both floating and submerged electrodes.

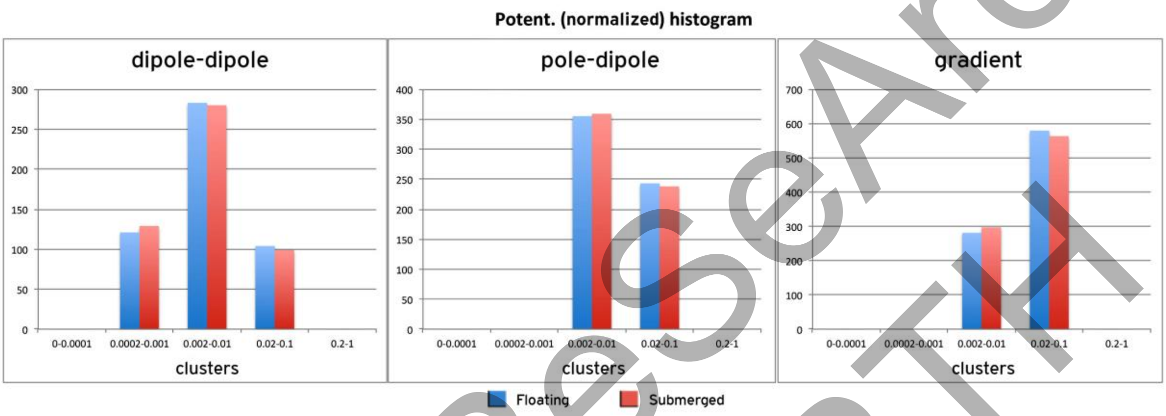

Figure 14. Histograms with normalized potential values for each array (dipole-dipole, pole-dipole and gradient) for floating and submerged electrodes.

Inversion results for floating electrodes (Figure 15, left panel) show that the protocol pole-dipole after 7 iterations with rms error 1.22%, reconstructed the targets (shown with letters 'A', 'B' and 'C') that have already been seen with diving at the depth of 2m below sea level with resistivity value of 5 ohm-m. Some additional smaller targets are also mapped that were not visible through diving. As seen the synthetic data, some artifacts are created during the inversion at the edges of the survey line and should be taken into account when dealing with field data. For that reason, we recommend the survey line to be longer than the target area in order not to have artifacts at the edges that can be confused as potential targets. For this specific area for practical reasons (the length of the cable) it was not possible to have longer survey line. Similar inversion results are shown when using protocol gradient after 7 iterations and rms error 1.87%, since the targets are reconstructed at the same position as pole-dipole.

The dipole-dipole protocol (after 7 iterations and with 1.16% rms error) is able to locate the targets but they are less visible due to the weaker signal to noise ratio. Also a resistive layer is located at the depth of 7m but it should be considered as an artifact due to the poor reconstruction of the deeper part of the dipole-dipole model.

When submerged electrodes are used (Figure 15, right panel), with protocol pole-dipole (after 7 iterations with rms error 1%) the targets are reconstructed slightly shifted downwards, following the results shown in the numerical simulation. Gradient array model shows comparable results with 2.33% rms error and 7 iterations having at the same relatively higher resistivity values than pole-dipole. When protocol dipole-dipole is used less artifacts are observed in relation to the floating model but the targets are more difficult to be distinguished. The rms error is 1.10% and the target resistivity values are less than 5 ohm-m.

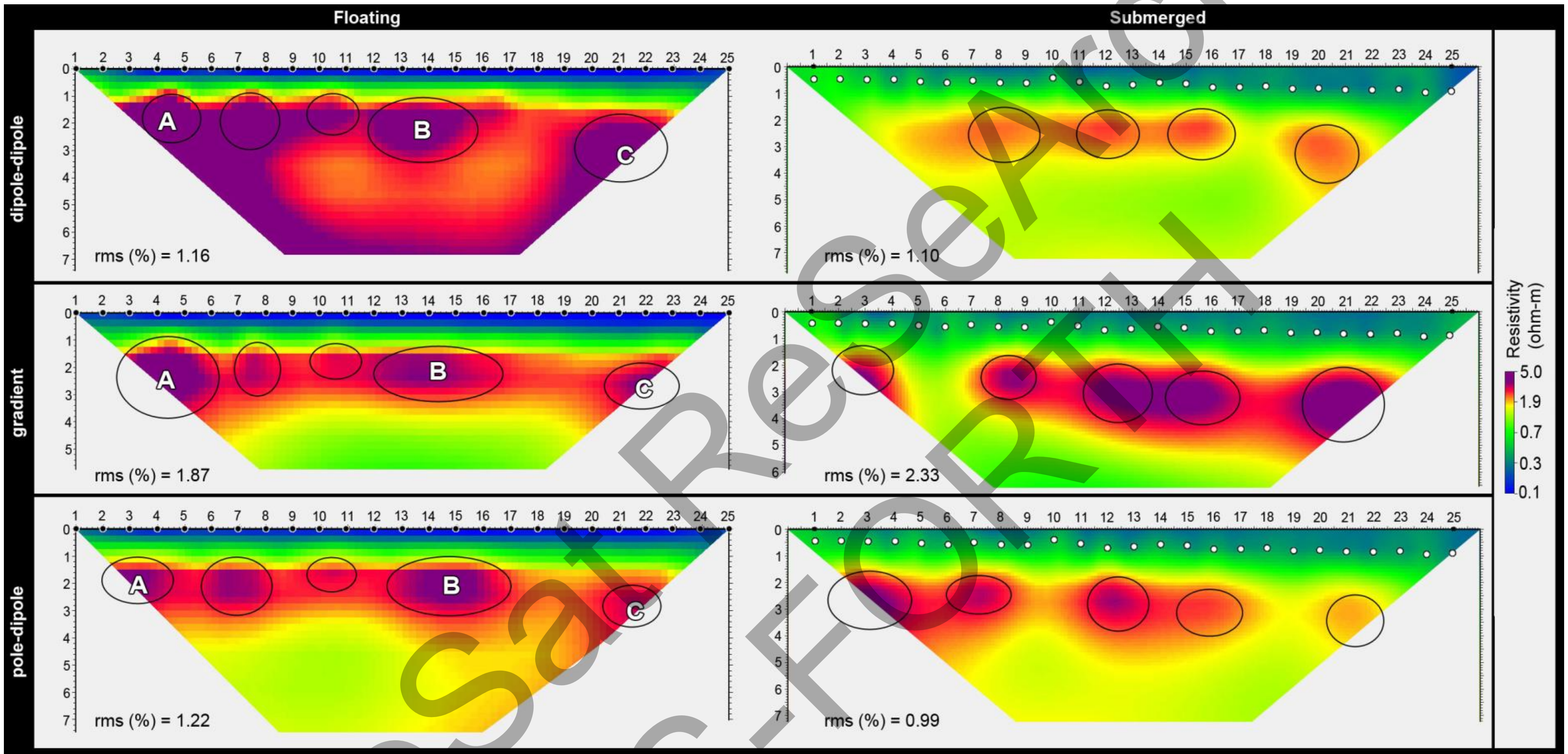

Figure 15. Inversion results with both floating (left) and submerged (right) electrodes using all protocols (dd, grd and pd). The archaeological targets are highlighted with black circles. Letters A, B and C indicate relics that are exposed from the sea bottom and can be easily seen.

CONCLUSIONS

This work examined the efficiency of Electrical Resistivity Tomography in mapping isolated archaeological targets in marine environments using both numerical simulations and validation with real data. The synthetic inversion results show that the targets simulating walls can be detected and among the tested arrays used, pole-dipole seems to have superior results in relation to gradient and dipole-dipole arrays.

Numerical modeling proposes a probe spacing half the smallest target dimension to ensure that archaeological features can be resolved. Floating and submerged survey modes can be used equally successfully in cases of relative shallow marine environments when the water depth doesn't exceed one meter. In deeper marine environments the submerged mode survey is recommended for outlining isolated targets.

In general it seems that pole-dipole and gradient arrays, both in floating and submerged survey modes, show strong resolving capabilities in mapping submerged cultural structures. The weak signal of dipole-dipole renders it inappropriate for outlining isolated targets in the shallow marine environments.

Valid 'a priori' information, in terms of the seawater resistivity and thickness, is important and can greatly improve the inversion results for the data captured with the submerged ERT mode. On the other hand erroneous information can cause severe distortions in the inversion ERT models and misleading interpretations.

The proposed methodology was applied in a field situation of a submerged archaeological site in Crete. Different electrode arrays (dipole-dipole, pole-dipole, gradient) and survey modes (floating vs. submerged) were tested along a line that crossed known submerged wall structures. The data analysis and results verified and enhanced the numerical modeling simulation thus establishing the effectiveness of the method.

In general this work shows the applicability, the potential as well as the constraints of the ERT in mapping isolated archaeological structures (e.g. walls or buildings) in shallow marine environments. These promising results can render ERT novella useful tool in the service of archaeological investigation of coastal and shallow marine sites. It can definitely integrated in wider archaeological projects in order to extract quantitative new information about submerged cultural material that is inaccessible to the standard mapping techniques.

ACKNOWLEDGEMENTS

This work was performed in the framework of the PEFYKA project within the KRIPIS Action of the GSRT. The project is funded by Greece and the European Regional Development Fund of the European Union under the NSRF and the O.P. Competitiveness and Entrepreneurship.

REFERENCES

Allen, D.A., 2007, Electrical conductivity imaging of aquifers connected to watercourses. PhD Thesis, University of technology Sidney, Australia.

Apostolopoulos, G., 2012. Marine resistivity tomography for coastal engineering applications in Greece. Geophysics, 77, B97-B105.

Baumgartner, F. and Christensen, N. B., 1998. Analysis and application of a non-conventional underwater geoelectrical method in Lake Geneva, Switzerland. Geophysical Prospecting, 46, 527-541.

Colombero C., Comina C., Gianotti F., Sambuelli L., 2014, Waterborne and on-land electrical surveys to suggest the geological evolution of a glacial lake in NW Italy. Journal of Applied Geophysics, vol. 105, pp. 191-202. - ISSN 0926-9851.

Hyoung-Seok Kwon, Jung-Ho Kim, Hee-Yoon Ahn, Jin-Sung Yoon, Ki-Seog Kim, Chi-Kwang Jung, Seung-Bok Lee, Toshihiro Uchida, 2005. Delineation of a fault zone beneath a riverbed by an electrical resistivity survey using a floating streamer cable, Exploration Geophysics, vol.36, p. 50-58.

Kim J.H, Yi M.J., 2010. 'DC2D_PRO', Geoelectrical Modeling and Inversion, User's Manual, Korea Institute of Geoscience and Mineral Resources, Korea.

Kim J.-H., Yi, M.-J.., Song, Y., Cho, S.J., Chung, S.H. and Kim, K.-S., 2002. DC Resistivity Survey to Image Faults Beneath a Riverbed: Symposium on the Application of

Geophysics to Engineering and Environmental Problems (SAGEEP 2002), 13IDA10, Las Vegas, USA.

Kim J.H., Tsourlos P., Yi. M.J., Karmis, P., 2014. Inversion of ERT data with a priori information using variable weighting factors. Journal of Applied Geophysics, 105, 1-9.

Lagabrielle, R., 1983. The effect of water on direct current resistivity measurement from sea, river or lake floor. Geoexploration, 21, 165-170.

Loke M.H., Lane J.W.L.Jr., 2004. Inversion of data from electrical resistivity imaging surveys in water-covered areas, Exploration Geophysics 35, 266-271

Marinatos S., 1926. The Excavation of Nirou Chani Crete *(in greek)*, Proceedings of the Archaeological Society, p.142-147.

Orlando L., 2013. Some considerations on electrical resistivity imaging for characterization of waterbed sediments, Journal of Applied Geophysics, .95, 77-89.

Passaro, S., 2010. Marine electrical resistivity tomography for shipwreck detection in very shallow water: a case study from Agropoli (Salerno, southern Italy). Journal of Archaeological Science 37, p.1989–1998.

Psomiadis D., Tsourlos P., Albanakis K., 2009. Electrical resistivity tomography mapping of beachrocks: Application to the island of Thassos (N. Greece), Environmental Earth Sciences, 59, p.233-240.

Rucker D.F., Noonan G.E., Greenwood W.JW, 2011. Electrical resistivity in support of geological mapping along the Panama Canal Engineering Geology, 117, 121-133, 2011.

Wynn J.C. and Grosz A.E., 2000. Induced-polarization – a tool for mapping titanium-bearing placers, hidden metallic objects, urban waste on and beneath the seafloor: Journal of Environmental and Engineering Geophysics, 5, 27–35.